J Therm Anal Calorim (2009) 97:879–884
DOI 10.1007/s10973-009-0173-6

Non-isothermal decomposition kinetics of $NiFe_2O_4$ nanoparticles synthesized using egg white solution route

Banjong Boonchom · Santi Maensiri

Received: 24 December 2008 / Accepted: 22 April 2009 / Published online: 19 June 2009

Abstract The thermal decomposition kinetics of nickel ferrite ($NiFe_2O_4$) precursor prepared using egg white solution route in dynamical air atmosphere was studied by means of TG with different heating rates. The activation energy (E_α) values of one reaction process were estimated using the methods of Flynn–Wall–Ozawa (FWO) and Kissinger–Akahira–Sunose (KAS), which were found to be consistent. The dependent activation energies on extent of conversions of the decomposition reaction indicate "multi-step" processes. XRD, SEM and FTIR showed that the synthesized $NiFe_2O_4$ precursor after calcination at 773 K has a pure spinel phase, having particle sizes of $\sim 54 \pm 29$ nm.

Keywords Thermal decomposition · Kinetic study · Characterization · Growth from solutions · Inorganic compounds · Nanomaterials · Magnetic materials

B. Boonchom
King Mongkut's Institute of Technology Ladkrabang, Chumphon Campus, 17/1 M. 6 Pha Thiew District, Chumphon 86160, Thailand

B. Boonchom
Department of Chemistry, Faculty of Science, King Mongkut's Institute of Technology Ladkrabang, Bangkok 10520, Thailand

S. Maensiri
Department of Physics, Faculty of Science, Small & Strong Materials Group (SSMG), Khon Kaen University, Khon Kaen 40002, Thailand

S. Maensiri (✉)
Integrated Nanotechnology Research Center (INRC), Khon Kaen University, Khon Kaen 40002, Thailand
e-mail: sanmae@kku.ac.th; santimaensiri@gmail.com

Introduction

Nickel ferrite ($NiFe_2O_4$) is one of the most important spinel ferrites. It has an inverse spinel structure showing ferrimagnetism that originates from magnetic moment of antiparrallel spins between Fe^{3+} ions at tetrahedral sites and Ni^{2+} ions at octahedral sites [1]. This material is technologically important and has been used in many applications including magnetic recording media and magnetic fluids for the storage and/or retrieval of information, magnetic resonance imaging (MRI) enhancement, catalysis, magnetically guided drug delivery, sensors, pigments, etc. [2]. Various methods have been developed to synthesize nanocrystalline $NiFe_2O_4$, including sonochemical process [3], citrate precursor techniques [4], co-precipitation [5], mechanical alloying [6], sol–gel [7], pulsed wire discharge [1], shock wave [8], reverse micelle [9], hydrothermal [10], and ultrasonically assisted hydrothermal process[11]. Among these established synthesis methods, it is still critical to find simple and cost effective routes to synthesize nanocrystalline $NiFe_2O_4$ by utilization of cheap, non-toxic and environmentally benign precursors. Most recently, our group reported the synthesis of $NiFe_2O_4$ nanoparticles by a simple method using Ni and Fe nitrates and freshly extracted egg white (ovalbumin) in an aqueous medium [12]. However, detailed thermal decomposition kinetics of the prepared $NiFe_2O_4$ precursor which is of interest for better under standing on the formation of $NiFe_2O_4$ by this method had not been investigated. Decomposition of solids is the subject of many kinetics studies. In many methods of kinetics estimation, isoconversional method is recommended as trustworthy way of obtaining reliable and consistent kinetic information [13, 14]. It is a 'model-free method', which involves measuring the temperatures corresponding to fixed values of the

extent of conversion (α) from experiments at different heating rates (β).

In the present study, we report on the thermal decomposition kinetics of the egg-white synthesized $NiFe_2O_4$ precursor. The formation of $NiFe_2O_4$ nanoparticles from the prepared $NiFe_2O_4$ precursor was followed by differential thermal analysis-thermogravimetry (TG-DTG/DTA), X-ray powder diffraction (XRD), Fourier transform-infrared (FT-IR) spectroscopy, and scanning electron microscopy (SEM). The kinetics analysis of the non-isothermal results for decomposition process of the prepared $NiFe_2O_4$ precursor was carried out using the isoconversional methods of Flynn–Wall–Ozawa (FWO) [15, 16] and Kissinger–Akahira–Sunose (KAS) [17–19], which was reported for the first time.

Experimental

Precursor and nanoparticles of $NiFe_2O_4$ were prepared using egg white solution route of which the detail is reported elsewhere [12]. This simple route has been previously used to prepare a plate-like clusters of CeO_2 nanocrystalline particles with particle size of 6–30 nm [20]. Thermal analysis measurements (thermogravimetry, TG; differential thermogravimetry, DTG; and differential thermal analysis, DTA) were carried out by a Pyris Diamond Perkin Elmer apparatus by increasing temperature from 323 to 873 K with the use of calcined α-Al_2O_3 powder as the standard reference. The experiments were performed in static air, at heating rates of 5, 10, 15, 20 and 25 K min^{-1}. The sample mass was kept 6.0–10.0 mg in alumina crucible without pressing. The structure and crystalline size of the prepared precursor and the sample calcined at 773 K were studied by X-ray powder diffraction using a D8 Advanced powder diffractometer (Bruker AXS, Karlsruhe, Germany) with CuKα radiation ($\lambda = 0.15406$ Å). The morphology of the calcined sample was examined with scanning electron microscope (LEO SEM VP1450) after gold coating. The room temperature FT-IR spectra were recorded in the range of 4,000–370 cm^{-1} with 8 scans on a Perkin-Elmer Spectrum GX FT-IR/FT-Raman spectrometer with the resolution of 4 cm^{-1} using KBr pellets (spectroscopy grade, Merck).

Results and discussion

Characterization

TG curves of the thermal decomposition of $NiFe_2O_4$ using egg white solution precursor at five heating rates are shown in Fig. 1. All curves are approximately in the same shape

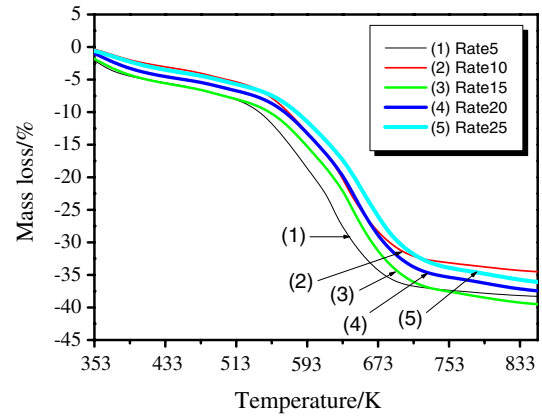

Fig. 1 TG curves of the $NiFe_2O_4$ precursor prepared using egg white solution at five heating rates of 5, 10, 15, 20 and 25 K min^{-1} in air

indicating that the mass loss is dependent of the heating rate. The TG curve in Fig. 1 shows a minor weight loss step from 323 K up to about 487 K and a major weight loss step from 487 K up to about 748 K. The minor weight loss is related to the loss of moisture and trapped solvent (water and carbon dioxide) while the major weight loss is due to the combustion of organic ovalbumin matrix. DTG-DTA curves of $NiFe_2O_4$ precursor at the heating rate of 10 K min^{-1} in air are shown in Fig. 2. The peak in the DTG curve closely corresponds to the mass loss observed on the TG trace. The mass retained is about 62% for all heating rates, compatible with the value expected for the formation of $NiFe_2O_4$, which is verified by XRD measurement (Fig. 3). The mass loss in the range of 478–748 K depends on the heating rate—the mass loss increases with the decreasing of the heating rate. On the DTA curve, the corresponding exothermic peaks at ~483, 585 and 645 K suggest that the thermal events are related to the burn-out of organic species associated in the precursor (the organic mass remained in ovalbumin), or the residual carbon. The temperature can be also determined from the TG curves and considered to be the minimum temperature needed for

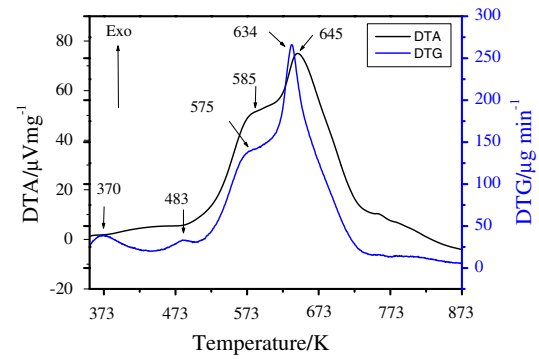

Fig. 2 DTG-DTA curves of the prepared $NiFe_2O_4$ precursor at heating rate of 10 K min^{-1} in air

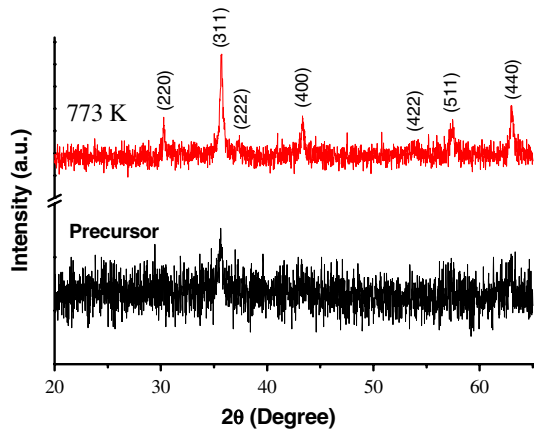

Fig. 3 The XRD patterns of the prepared $NiFe_2O_4$ precursor (**a**) and $NiFe_2O_4$ nanoparticles calcined in air at 773 K (**b**)

the calcination process. Thus, to obtain $NiFe_2O_4$ nanoparticles, the $NiFe_2O_4$ precursor sample was calcined in air at 773 K for 3 h in the box furnace.

The XRD patterns of the precursor and calcined $NiFe_2O_4$ samples are shown in Fig. 3. All of the detectable peaks are indexed as the $NiFe_2O_4$ with inverse spinel structure as shown in the standard data (JCPDS: 10-0325). No diffraction peaks of other impurities such as α-Fe_2O_3, NiO were observed. The average crystallite sizes of $NiFe_2O_4$ samples were calculated from X-ray line broadening of the reflections of (311), (400), (511) and (440) using Scherrer's equation ($D = \lambda k/(\beta\cos\theta)$, where λ is the wavelength of the X-ray radiation, k is a constant taken as 0.89, θ is the diffraction angle and β is the full width at half maximum (FWHM) [21]), and were found to be 54 ± 29 nm. The lattice parameter (a) calculated from the XRD spectrum was $a = 0.83274 \pm 0.00013$ nm.

The morphology of the calcined $NiFe_2O_4$ sample is shown in Fig. 4. The calcined $NiFe_2O_4$ sample contains agglomerated nanoparticles with particle size of ~30–80 nm. This is in agreement with the estimated value obtained from XRD results.

The formation of spinel $NiFe_2O_4$ structure in the calcined $NiFe_2O_4$ sample was further supported by FT-IR spectra (Fig. 5). Here we consider two ranges of the absorption bands: 4,000–1,000 cm^{-1} and 1,000–370 cm^{-1} as suggested by previous published work [12, 22–24]. In the range of 1,000–100 cm^{-1}, two main metal-oxygen bands at ~590 and 397 cm^{-1} were observed in the FTIR spectrum of the 773 K-calcined $NiFe_2O_4$ sample (Fig. 3b). These two bands are usually assigned to vibration of ions in the crystal lattices [25]. The band at ~590 cm^{-1}corresponds to intrinsic stretching vibrations of the metal at the tetrahedral site (Fe ↔ O), whereas the band at ~397 cm^{-1} is assigned to octahedral-metal stretching (Ni ↔ O) [26, 27].

Kinetics studies

Dehydration of crystal hydrates is a solid-state process of the type [27, 28]:

$$A(\text{solid}) \rightarrow B(\text{solid}) + C(\text{gas}).$$

The kinetics of such reactions is described by various equations taking into account the special features of their mechanisms. The reaction rate can be expressed through the degree of conversion α (the ratio between the weight loss at moment t and the total weight loss by the end of dehydration) and its temperature dependence:

$$\frac{d\alpha}{dt} = k(T)f(\alpha) \quad (1)$$

where t is the time, T is the temperature. α is the extent of conversion which is given by

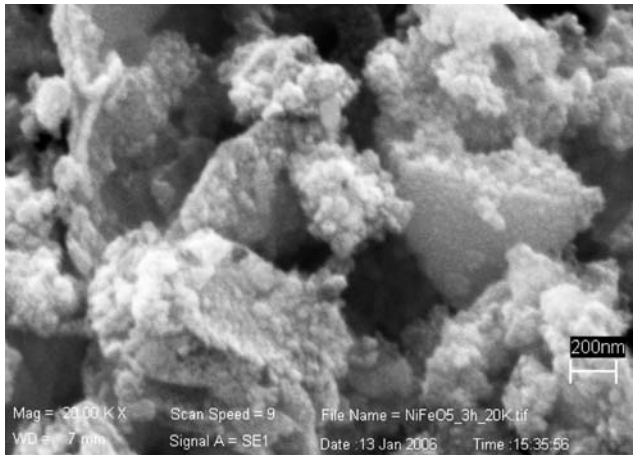

Fig. 4 SEM micrograph of the $NiFe_2O_4$ nanoparticles calcined in air at 773 K

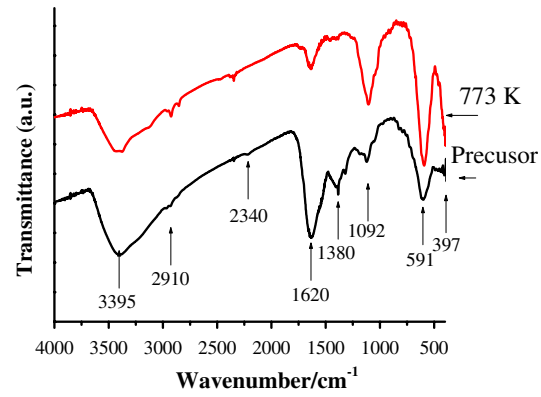

Fig. 5 FT-IR spectra of the prepared $NiFe_2O_4$ precursor (**a**) and $NiFe_2O_4$ nanoparticles calcined in air at 773 K (**b**)

$$\alpha = \frac{Wi - Wt}{Wi - Wf} \tag{2}$$

where W_i, W_t and W_f are the initial, actual and final weight of the sample, respectively, and $f(\alpha)$ is the reaction model. The explicit temperature dependence of the rate constant is introduced by replacing $k(T)$ with the Arrhenius equation, which gives

$$k = A\exp\left(-\frac{E}{RT}\right) \tag{3}$$

where A (the pre-exponential factor) and E (the activation energy) are the Arrhenius parameters and R is the gas constant (8.314 J mol^{-1} K^{-1}). The Arrhenius parameters, together with the reaction model, are sometimes called the kinetic triplet.

Two isoconversional kinetic methods are used in this paper to calculate activation energy (E_α). These methods have been recommended by International Confederation of Thermal Analysis Calorimetry (ICTAC) due to the fact that they allow the E value to be independently obtained [29, 30]. These equations are as follows:

FWO equation [15, 16]:

$$\ln\beta = \log\left(\frac{AE_\alpha}{Rg(\alpha)}\right) - 5.3305 - 1.0516\left(\frac{E_\alpha}{RT}\right) \tag{4}$$

KAS equation [17–19] (adopted from ASTM 698-79 [31]):

$$\ln\left(\frac{\beta}{T^2}\right) = \ln\left(\frac{AE_\alpha}{Rg(\alpha)}\right) - \left(\frac{E_\alpha}{RT}\right) \tag{5}$$

$g(\alpha) = \int_0^\alpha \frac{d\alpha}{f(\alpha)}$ is the integral form of the $f(\alpha)$, which is the reaction model that depends on the reaction mechanism.

At the constant condition of other parameters, the TG curves for dehydration of the prepared $NiFe_2O_4$ precursor in air at various heating rates of 5, 10, 15, 20 and 25 K min^{-1} are shown in Fig. 1. According to an isoconversional method, the basic data of α and T collected from Fig. 1. According to the above-mentioned equations, the plots of ln β versus 1000/T (FWO) and ln β/T^2 versus 1000/T (KAS) corresponding to different conversions α can be obtained by a linear regress of least-square method, respectively. The FWO and KAS analysis results taken from the four TG measurements below 693 K are presented in Figs. 6 and 7, respectively. The activation energies E_α can be calculated from the slopes of the straight lines with better linear correlation coefficient (>0.99). The activation energies are calculated at heating rates of 5, 10, 15, 20 and 25 K min^{-1} via the FWO and KAS methods in the α ranges of 0.2 to 0.8, and are tabulated in Table 1. The average activation energies calculated by FWO and KAS methods are obtained to be 227.31 and 221.98 kJ mol^{-1}, respectively. It is seen that the activation energy values calculated by the KAS method are close to that obtained by FWO method. If E_α values are independent of α, the decomposition may be a simple reaction, [20–22] while the dependence of E_α on α should be interpreted in terms of multi-step reaction mechanisms [14–16]. The activation energies depend on α, so we draw a conclusion that the

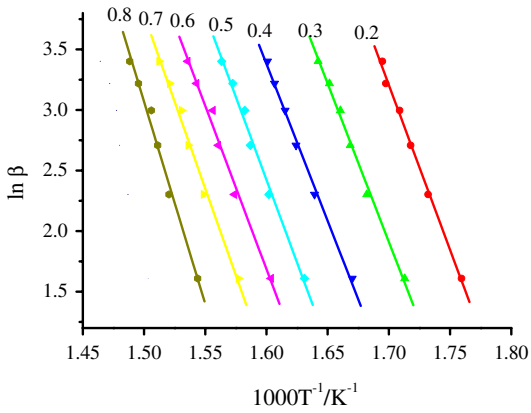

Fig. 6 FWO analysis of five TG measurements below 693 K

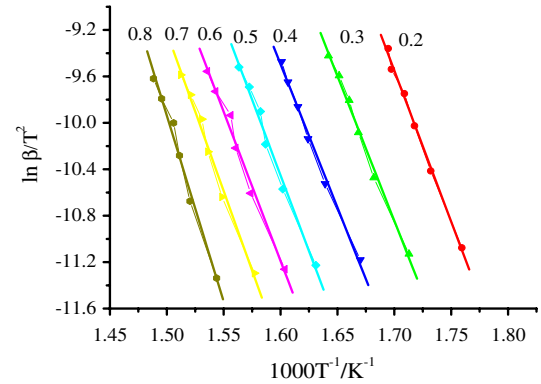

Fig. 7 KAS analysis of five TG measurements below 693 K

Table 1 Activation energies (E_α) versus correlation coefficient (r^2) calculated by FWO and KAS methods for the decomposition of the prepared $NiFe_2O_4$ precursor

α	FWO method		KAS method	
	E_α/kJ mol^{-1}	r	E_α/kJ mol^{-1}	r
0.2	215.13	0.9982	216.60	0.998
0.3	206.63	0.9971	207.39	0.9968
0.4	205.00	0.9977	205.41	0.9975
0.5	216.19	0.9951	216.94	0.9946
0.6	213.21	0.9936	213.62	0.993
0.7	226.50	0.995	227.42	0.9946
0.8	263.87	0.9938	266.52	0.9933
Average	227.31 ± 20.20	0.9958	221.98 ± 20.92	0.9954

decomposition reaction process of the prepared $NiFe_2O_4$ precursor is a complex kinetic mechanism (successive or parallel reactions, reversible reaction, etc.). This results shows that the importance of the isoconversional methods consists just in their capacity to evaluate the E versus α without the knowledge of the kinetic model ($g(\alpha)$).

Kinetic analysis of the oxalate decomposition steps in NiFe mixture for the formation of $NiFe_2O_4$ has been studied by Gabal [31–35]. He reported two steps of kinetics decomposition for FeC_2O_4 and NiC_2O_4, which appear in the second and third steps, respectively. The reported kinetic model of the oxalate decomposition reactions were the three-dimensional phase boundary (R_3) model. The reported activation energies using the Coats–Redfern method for the thermal decomposition of FeC_2O_4 and NiC_2O_4 were 140 and 250 kJ mol^{-1}, respectively. These results are different from the present study, and the kinetic analysis in our work confirms that lower calcination temperature than that report in literature [35] is possible for the $NiFe_2O_4$ precursor synthesized by egg white solution route. This work also confirms that the kinetic triplet values (A, E and kinetic model) for $NiFe_2O_4$ are strongly dependent of preparation method.

Conclusions

The $NiFe_2O_4$ precursor prepared by using egg white solution decomposes in one well defined step by starting after 478 K and the final product is $NiFe_2O_4$. The final product is confirmed by XRD data, FTIR and SEM techniques. Kinetic analysis from non-isothermal TG applying model-fitting method results a single value of E on the different α which can be assigned to multi-step reaction. The activation energies calculated for the decomposition of the prepared $NiFe_2O_4$ precursor using different models and techniques were found to be inconsistent. This indicates that the activation energy of decomposition is dependent on process and the nature of non-isothermal methods as well as TGA results. The data of kinetics play an important role in theoretical study, application development and industrial production of a compound as a basis of theoretical. Additionally, various scientific and practical problems involving the participation of solid phases can be solved.

Acknowledgments The authors would like to thank the Faculty of Science SEM Unit for providing SEM facilities, the Department of Chemistry, Khon Kaen University for providing TG/DTG/DTA and FTIR facilities, and the Department of Environmental Engineering, Faculty of Engineering for providing XRD facilities. We are grateful to C. Masingboon for his assistance. This work is partially supported by The National Nanotechnology Center (NANOTEC), NSTDA, Ministry of Science and Technology, Thailand, through its program of Center of Excellence.

References

1. Kinemuchi Y, Ishizaka K, Suematsu H, Jiang W, Yatsui K. Magnetic properties of nanosize $NiFe_2O_4$ particles synthesized by pulsed wire discharge. Thin Solid Films. 2002;407:109–13.
2. Sugimoto M. The past, present, and future of ferrites. J Am Ceram Soc. 1999;82:269–79.
3. Shafi KVPM, Koltypin Y, Gedanken A, Prozorov R, Balogh J, Lendvai J, et al. Sonochemical preparation of nanosized amorphous $NiFe_2O_4$ particles. J Phys Chem B. 1997;101:6409–14.
4. Prasad S, Gajbhiye NS. Magnetic studies of nanosized nickel ferrite particles synthesized by the citrate precursor technique. J Alloys Compd. 1998;265:87–92.
5. Yang JM, Tsuo WJ, Yen FS. Preparation of ultrafine nickel ferrite powders using mixed Ni and Fe tartrates. J Solid State Chem. 1999;145:50–7.
6. Shi Y, Ding J, Liu X, Wang J. $NiFe_2O_4$ ultrafine particles prepared by co-precipitation/mechanical alloying. J Magn Magn Mater. 1999;205:249–54.
7. Chen D-H, He X-R. Synthesis of nickel ferrite nanoparticles by sol–gel method. Mater Res Bull. 2001;36:1369–77.
8. Liu J, He H, Jin X, Hao Z, Hu Z. Synthesis of nanosized nickel ferrites by shock waves and their magnetic properties. Mater Res Bull. 2001;36:2357–63.
9. Kale A, Gubbala S, Misra RDK. Magnetic behavior of nanocrystalline nickel ferrite synthesized by the reverse micelle technique. J Magn Magn Mater. 2004;277:350–8.
10. Zhou J, Ma J, Sun C, Xie L, Zhao Z, Tian H. Low-temperature synthesis of $NiFe_2O_4$ by a hydrothermal method. J Am Ceram Soc. 2005;88:3535–7.
11. Meskin PE, Ivanov VK, Barantchikov AE, Churagulov BR, Tretyakov YD. Ultrasonically assisted hydrothermal synthesis of nanocrystalline ZrO_2, TiO_2, $NiFe_2O_4$ and $Ni_{0.5}Zn_{0.5}Fe_2O_4$ powders. Ultrason Sonochem. 2006;13:47–53.
12. Maensiri S, Masingboon C, Boonchom B, Seraphin S. A simple route to synthesize nickel ferrite ($NiFe_2O_4$) nanoparticles using egg white. Scripta Mater. 2007;56:797–800.
13. Budrugeac P, Segal E. Applicability of the Kissinger equation in thermal analysis. J Therm Anal Calorim. 2007;88:703–7.
14. Vlase T, Vlase G, Brita N, Doca N. Comparative results of kinetic data obtained with different methods for complex decomposition steps. J Therm Anal Calorim. 2007;88:631–5.
15. Ozawa T. New method of analyzing thermogravimetric data. Bull Chem Soc Jpn. 1965;38:1881–6.
16. Loiţescu A, Vlase G, Vlase T, Doca N. Thermal behaviour of some industrial and food dyes. J Therm Anal Calorim. 2007;88:121–5.
17. Kissinger HE. Reaction kinetics in differential thermal analysis. Anal Chem. 1957;29:1702–6.
18. Zhao MS, Song ZP. Synthesizing kinetics and characteristics for spinel $LiMn_2O_4$ with the precursor using as lithium-ion battery cathode material. J Power Source. 2007;164:822–8.
19. Lu Z, Yang L, Guo Y. Thermal behavior and decomposition kinetics of six electrolyte salts by thermal analysis. J Power Source. 2006;156:555–9.
20. Maensiri S, Masingboon C, Laokul P, Jareonboon W, Promarak V, Anderson PL, et al. Egg white synthesis and photoluminescence of platelike clusters of CeO_2 nanoparticles. Cryst Growth Des. 2007;7:950–55.
21. Cullity BD, Stock SR. Elements of X-ray diffraction. 3rd ed. Englewood Cliffs, NJ: Prentice-Hall; 2001.
22. Kamnev AA, Risti M. Fourier transform far-infrared spectroscopic evidence for the formation of a nickel ferrite precursor in binary Ni(II)–Fe(III) hydroxides on coprecipitation. J Mol Struct. 1997;408–409):301–4.

23. Chen D, Chen D, Jiao X, Zhao Y, He M. Hydrothermal synthesis and characterization of octahedral nickel ferrite particles. Powder Technol. 2003;133:247–50.
24. Mouallem-Bahout M, Bertrand S, Pena O. Synthesis and characterization of $Zn_{1-x}Ni_xFe_2O_4$ spinels prepared by a citrate precursor. J Solid Sate Chem. 2005;178:1080–6.
25. Brabers VAM. Infrared spectra of cubic and tetragonal manganese ferrites. Phys Stat Sol. 1969;33:563–72.
26. Waldron RD. Infrared spectra of ferrites. Phys Rev. 1955; 99:1727–35.
27. Vlaev LT, Nikolova MM, Gospodinov GG. Non-isothermal kinetics of dehydration of some selenite hexahydrates. J Solid State Chem. 2004;177:2663–9.
28. Vyazovkin S. A unified approach to kinetic processing of non-isothermal data. Int J Chem Kinet. 1996;28:95–101.
29. Brown ME, Maciezewski M, Vyazovkin S, Nomen R, Sempere J, Burnham A, et al. Computational aspects of kinetic analysis. Part A: the ICTAC kinetics project-data, methods and results. Thermochim Acta. 2000;355:125–43.
30. Burnham AK. Computational aspects of kinetic analysis. Part D: the ICTAC kinetics project—multi-thermal-history model-fitting methods and their relation to isoconversional methods. Thermochim Acta. 2000;355:165–70.
31. ASTM E698–79. Standard test method for Arrhenius kinetic constants for thermally unstable materials. Philadelphia: ASTM; 1984.
32. Budrugeac P. The Kissinger law and the IKP method for evaluating the non-isothermal kinetic parameters. J Therm Anal Calorim. 2007;89:143–51.
33. Gabal MA. Kinetics of the thermal decomposition of CuC_2O_4–ZnC_2O_4 mixture in air. Thermochim Acta. 2003;402:199–208.
34. Singh BK, Sharma RK, Garg BS. Kinetics and molecular modeling of biologically active glutathione complexes with lead(II) ions. J Therm Anal Calorim. 2006;84:593–60.
35. Vlaev LT, Georgieva VG, Genieva SD. Products and kinetics of non-isothermal decomposition of vanadium(IV) oxide compounds. J Therm Anal Calorim. 2007;88:805–12.